






Accurate standard siren cosmology with joint gravitational-wave and γ -ray burst observations

Michele Mancarella ^{1,2,3,*} Francesco Iacovelli ⁴ Stefano Foffa ⁴ Niccolò Muttoni ⁴ and Michele Maggiore ⁴

¹*Aix-Marseille Univ., Université de Toulon, CNRS, CPT, Marseille, France*

²*Dipartimento di Fisica “G. Occhialini”, Università degli Studi di Milano-Bicocca, Piazza della Scienza 3, 20126 Milano, Italy*

³*INFN, Sezione di Milano-Bicocca, Piazza della Scienza 3, 20126 Milano, Italy*

⁴*Département de Physique Théorique & Gravitational Wave Science Center (GWSC), Université de Genève, 24 quai Ernest Ansermet, 1211 Genève 4, Switzerland*

(Dated: May 6, 2024)

Joint gravitational-wave and γ -ray bursts (GRB) observations are among the best prospects for standard siren cosmology. However, the strong selection effect for the coincident GRB detection, which is possible only for sources with small inclination angles, induces a systematic uncertainty that is currently not accounted for. We show that this severe source of bias can be removed by inferring the a-priori unknown electromagnetic detection probability directly from multimessenger data. This leads at the same time to an unbiased measurement of the Hubble constant, to constrain the properties of GRB emission, and to accurately measure the viewing angle of each source. Our inference scheme is applicable to real data already in the small-statistics regime, a scenario that might become reality in the near future. Additionally, we introduce a novel likelihood approximant for GW events which treats the dependence on distance and inclination as exact.

Introduction. Gravitational waves are rapidly establishing as a new pillar of concordance cosmology [1]. A Hubble diagram can be constructed with luminosity distance measurements from gravitational-wave (GW) events in conjunction with redshift determinations [2]. The detection of a few to tens “bright sirens”, following GW170817 [3–5], can lead to an independent percent-level measurement of the Hubble constant H_0 [6–8], required to set the strong inconsistency between local [9] and CMB [10] measurements. With such precision, systematics will start playing a prominent role and prevent solving the Hubble tension unless properly accounted for – in particular, calibration uncertainty [11, 12], peculiar velocities corrections [13–15], and the EM selection effects [16].

The latter is the dominant source of bias when the counterpart is a short γ -ray burst (GRB) [16], which is observed only if the angular momentum of the binary is aligned with the line of sight, i.e. at small inclination. Since inclination and luminosity distance are inherently correlated in the GW waveform, with the correlation becoming stronger for small viewing angles, neglecting this effect leads to a strong bias on H_0 [16]. Knowing a priori the GRB emission mechanism, we could impose a prior on the inclination, but the limited knowledge of these phenomena makes this impossible. Independent measurements of the inclination from the observation of jet motions with Very Long Baseline Interferometry (VLBI) can help breaking the distance–inclination correlation [17–20], but these are not always guaranteed [21] and are themselves subject to modeling systematics [16]. Recently, proposals for mitigating the bias in absence of direct information on the inclination and on the GRB emission were put forward. These rely on estimating the EM

selection effect from a larger sample of BNS without counterparts [22, 23].

In this work, we instead propose to remove the bias by determining the EM selection function *solely from the joint sample of GW+GRB observations*. This scheme can be applied even with just two multimessenger events, in which case we find that neglecting the EM selection bias can lead to a $\mathcal{O}(10\%)$ shift of the posterior peak for H_0 . This could happen already during currently planned runs of the LVK collaboration [24]. As for a larger number of events, the bias can reach the $\sim 3\sigma$ ($\sim 2\sigma$) level for $\mathcal{O}(50)$ ($\mathcal{O}(10)$) detections, making the correction crucial. Our implementation can be directly applied to real data, demonstrated with a proof of principle application to GW170817.

Statistical formulation. We model the problem with a hierarchical Bayesian approach [25–27]. We consider a set of N_{obs} events with single-event detector-frame parameters $\{\theta_i\}_{i=1}^{N_{\text{obs}}}$ and data $\mathcal{D} = \{\mathcal{D}_{\text{GW}}^i, \mathcal{D}_{\text{EM}}^i\}_{i=1}^{N_{\text{obs}}}$. The EM data consist only in a redshift measurement for each event, following the identification of the host galaxy from the GRB. We instead remain agnostic to the data behind the detection of the GRB and only use the fact that such detection happened. For clarity, we introduce a set of boolean variables $\{\text{det}_{\text{GW}}^i, \text{det}_{\text{EM}}^i\}_{i=1}^{N_{\text{obs}}}$ where $\text{det}^i = 1$ if the event is detected and 0 otherwise. We assume that the GW catalog is obtained with a selection cut which is a known, deterministic function of the observed data only, as customary in hierarchical Bayesian analyses. On the other hand, the EM detections are also subject to a strong selection effect, but their selection function is not known a priori, since we do not know the mechanism behind GRB emission. Moreover, the possibility of measuring one source parameter – the redshift – depends on another one – the inclination – which is not directly measured. This introduces a dependence of the selection function

* mancarella@cpt.univ-mrs.fr

on the (also unknown) single event parameters θ . More specifically, we will model the EM detection probability, denoted by $P(\text{det}_{\text{EM}}^i|\theta_i, \lambda_{\text{EM}})$, as a function of the inclination angle ι and on the luminosity distance d_L (for the usual scaling of the flux with d_L^{-2}) with universal hyperparameters λ_{EM} describing the GRB jet structure and the GRB detection threshold.¹ We do not know the parameters λ_{EM} a priori, but we can infer them from the GW and redshift data and, crucially, from the information that the counterpart has been detected, i.e. $\text{det}_{\text{EM}}^i = 1$ for each event in the catalog.

The joint posterior on $\{\lambda, \{\theta_i\}\}$ can be written as

$$p(\lambda, \{\theta_i\} | \{\mathcal{D}_{\text{GW}}^i\}, \{\mathcal{D}_{\text{EM}}^i\}, \{\text{det}_{\text{GW}}^i\}, \{\text{det}_{\text{EM}}^i\}) \propto \frac{\pi(\lambda)}{P(\text{det}|\lambda)^{N_{\text{obs}}}} \times \prod_{i=1}^{N_{\text{obs}}} \mathcal{L}(\mathcal{D}_{\text{GW}}^i|\theta_i) \mathcal{L}(\mathcal{D}_{\text{EM}}^i|\theta_i, \lambda_c) \quad (1) \\ \times p_{\text{pop}}(\theta_i|\lambda) P(\text{det}_{\text{EM}}^i|\theta_i, \lambda_{\text{EM}}).$$

A derivation and detailed discussion of this posterior is given in App. A.² In Eq. (1), $p_{\text{pop}}(\theta_i|\lambda)$ is the probability of a source to have parameters θ_i given hyperparameters λ , $\lambda_c = \{H_0, \Omega_{m,0}\}$ are the cosmological parameters, $\mathcal{L}(\mathcal{D}_{\text{GW}}^i|\theta_i)$ and $\mathcal{L}(\mathcal{D}_{\text{EM}}^i|\theta_i, \lambda_c)$ are the GW and EM likelihoods, $\pi(\lambda)$ is the prior on hyperparameters, and $P(\text{det}|\lambda)$ denotes the fraction of detectable events [26]. This term contains both the GW and EM selection effects, with the latter given by $P(\text{det}_{\text{EM}}^i|\theta_i, \lambda_{\text{EM}})$.

The key difference between Eq. (1) and the standard hierarchical Bayesian posterior in GW population studies is the presence of the term $P(\text{det}_{\text{EM}}^i|\theta_i, \lambda_{\text{EM}})$ at the numerator. A similar contribution is not present for GW data because detectability is a property of data only, which allows us to write $\mathcal{L}(\text{det}_{\text{GW}}^i|\mathcal{D}_{\text{GW}}^i|\theta_i) = P(\text{det}_{\text{GW}}^i|\mathcal{D}_{\text{GW}}^i)\mathcal{L}(\mathcal{D}_{\text{GW}}^i|\theta_i) = \mathcal{L}(\mathcal{D}_{\text{GW}}^i|\theta_i)$, where the first equality follows from the composition of probabilities and the second from the fact that for detected events $P(\text{det}_{\text{GW}}^i|\mathcal{D}_{\text{GW}}^i) = 1$. A similar simplification does not hold for the EM likelihood due to the discussed dependence of the detection probability on θ_i and λ_{EM} . The interpretation of the detection probability $P(\text{det}_{\text{EM}}^i|\theta_i, \lambda_{\text{EM}})$ in Eq. (1) is that this term will reshape the GW likelihood essentially acting as a modification of the prior [30, 31] carrying information about the fact that the detection of the GRB emission preferentially selects small viewing angles. This breaks the distance–inclination correlation of each individual GW event likelihood leading to an unbiased estimate of H_0 (as well as of other cosmological parameters) and to the reconstruction of the maximum viewing angle.

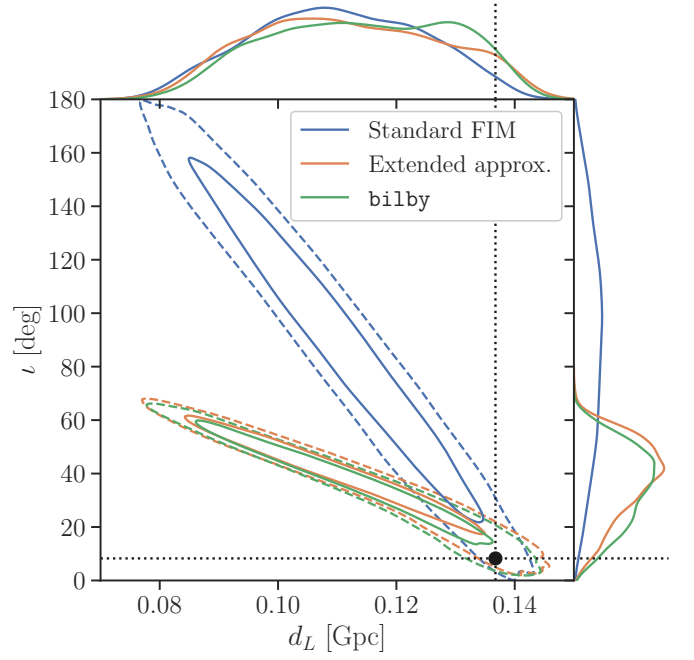


Fig. 1. Posterior probability in the distance–inclination plane for the highest SNR source in the simulations used for the results of this work. Orange contours are obtained using our new likelihood approximant which encodes the exact dependence of the likelihood on d_L and ι . Blue contours show for comparison the Fisher matrix approximation, which is inaccurate for sources at low inclination. Green contours are obtained from a Bayesian parameter estimation with **parallel bilby**.

A new GW likelihood approximant. The GW data are usually given, for each event i , in terms of samples from the posterior probability $p(\theta_i|\mathcal{D}_{\text{GW}}^i) \propto \mathcal{L}(\mathcal{D}_{\text{GW}}^i|\theta_i)\pi(\theta_i)$ where $\pi(\theta_i)$ is the prior used to analyze the data. However, full Bayesian simulations are quite expensive, especially for BNS, and are often circumvented by resorting to the Fisher Information Matrix (FIM) approximation, i.e. a Gaussian approximation of the likelihood around its peak [32]. This however fails precisely in the corner of the parameter space which is relevant for GRBs, i.e. at small or vanishing inclination angle [33, 34], regardless of possible regularizations or of the use of priors [32–35].

For this study, we develop a new likelihood approximant that treats the likelihood in the subspace $\{d_L, \iota\}$ as exact, while resorting to the FIM in the rest of the parameter space. This extends existing approaches, e.g. [36–39]. The result is given in terms of a simple combination of FIM elements, computable with open-source packages [35, 40, 41]. We also introduce a second extension of the FIM approximation, in order to properly encode the effects of noise fluctuations [31]. This is based on an expansion around the point maximizing the likelihood in presence of noise, which we obtain numerically from an explicit realization of the noise in the frequency domain. The procedure is described in detail App. B and the result for the likelihood can be found in Eq. (B10).

¹We assume that the viewing angle of the GRB is the same as (or a good proxy of) ι in the GW signal, and that it has a universal structure (see e.g. [28, 29]).

²See also [30] for a similar discussion in the context of GW data only.

Fig. 1 shows posterior contours in the distance–inclination plane for the highest SNR source in our simulation, obtained with our extended likelihood approximant (orange), compared to the FIM (blue), and, as proof of the validity of the extended approximant, to a full Bayesian simulation with `parallel bilby` [42, 43] (green). We see that the FIM completely mismodels the shape of the likelihood, while the agreement between our approximant and the full likelihood is excellent. The biased reconstruction of the marginal distance posterior in Fig. 1 is a consequence of the small inclination of the source and is therefore intrinsic to any multimessenger event with a GRB, and the origin of the systematic uncertainty on H_0 .³

This simulation scheme is indispensable for studies of third-generation (3G) detectors, for which an efficient and scalable Bayesian inference sampling tool is still missing (but see [44–47] for recent progress), while detection rates are expected to be large [33, 48].

Case study. We now illustrate the method on a simple yet realistic example for the current generation of GW and EM experiments, namely, a LIGO–Virgo–KAGRA–LIGO India (LVKI) network [49–53] and Fermi–GBM [54].

We simulate a population of BNS with a Madau–Dickinson profile for the merger rate [55], a Gaussian mass distribution, and inclinations uniformly distributed on the sphere. We assume an LVKI network at design sensitivity with a 100% duty cycle and threshold on the observed SNR $\rho_{\text{obs}} \geq 12$ [53]. For the EM detection model, we assume that the GRB jet has a Gaussian-shaped profile with amplitude A_0 and half-opening ι_c , compatible with the multimessenger analysis of GW170817 [56] (see Eq. (C1)). We consider an event detected if the flux exceeds the Fermi–GBM–like sensitivity of $F_{\text{th}} = 2 \times 10^{-7} \text{ erg cm}^{-2} \text{ s}^{-1}$ [54]. This model predicts a maximum viewing angle $\Theta_{\text{max}} = \min\{\iota_{\text{max}}, 180^\circ - \iota_{\text{max}}\}$ of order $\Theta_{\text{max}} \sim 11^\circ$ (0.2 rad) in the redshift range of interest for our sample (see Fig. 4 below). Our simulated dataset consists of a set of samples from the posterior $p(\theta_i | \mathcal{D}_{\text{GW}}^i) \propto \mathcal{L}(\mathcal{D}_{\text{GW}}^i | \theta_i) / \pi(\theta_i)$ obtained with the likelihood approximant introduced before, and a redshift measurement with uncertainty $\sigma_z = 10^{-3}$ for each GW event. We sample Eq. (1) in the high-dimensional space of $\lambda, \{\theta_i\}$ using PyMC [57] and the Hamiltonian Monte Carlo–based scheme NUTS [58, 59]. The hyperparameters λ include cosmology, mass, and redshift distributions, together with the parameters $\lambda_{\text{EM}} = \{A_0, \iota_c, F_{\text{th}}\}$ describing the EM detection probability. Tab. I in App. C contains a summary, with the same appendix containing a detailed description of the population model, of the mock catalog and of the inference scheme.

Fig. 2 shows the effect of neglecting (red lines) and inferring (green lines) the EM detection probability on

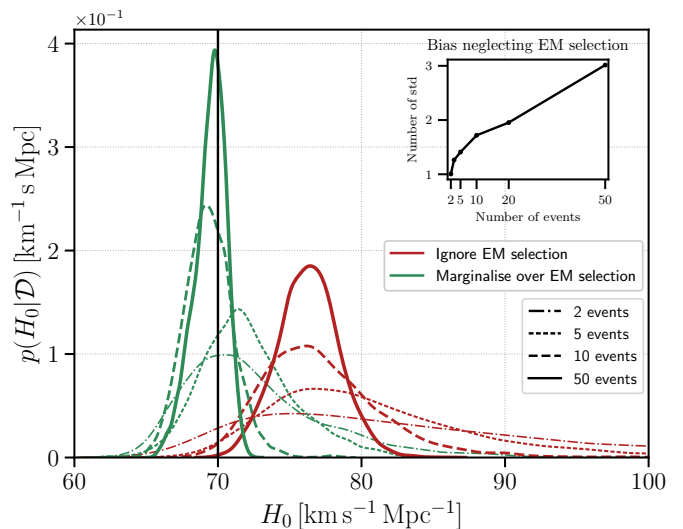


Fig. 2. Marginal posterior probability on H_0 , without (red) and with (green) the inclusion of the EM detection probability. Different line styles correspond to a different number of events analyzed, as in the legend. The inset shows the bias on the measurement when neglecting the EM selection probability.

the posterior probability on H_0 , marginalized over all the remaining hyperparameters and individual event parameters, for 2, 5, 10 and 50 events. When neglecting the EM detection probability a non-negligible ($\sim 7 - 10\%$) shift of the peak is already visible for 2 events, remaining stable as the number of detections increases. The simultaneous fit of the EM selection function can remove the bias as far as ≥ 2 events are included in the analysis. Of course, for low statistics, the bias is partially compensated by the large statistical uncertainty. The inset in Fig. 2 quantifies the bias as the ratio between the shift of the posterior peak from the injected value and the half 68.3% Highest Density Interval, which we denote by σ being this quantity the standard deviation in the Gaussian case. This reaches the $\sim 2\sigma$ level between 10 and 20 events and $\sim 3\sigma$ for 50 events. We conclude that while for low detection rates the shift of the peak could be somewhat compatible with a noise fluctuation, only the inclusion of the EM selection effect can ensure a robust measurement. For a larger number of detections, as might be expected in a few years of O4–O5 observations [60] and should be expected for 3G detectors [48], the bias is statistically significant and must be corrected.

Fig. 3 shows the correlation between H_0 and the half-width of the jet ι_c , when the EM detection probability is inferred from the data. In particular, for $\gtrsim 10$ events, large values of ι_c ($\gtrsim 5^\circ$) are excluded. This shows that adopting the strategy of putting a prior on the inclination of single events without inferring it from data can lead to a biased estimate of H_0 .

Furthermore, our inference scheme allows us to reconstruct the posterior probabilities of individual source parameters for each event, properly reweighted by the

³The bias is further exacerbated by the use of a prior on inclination flat in $\cos \iota$, following the assumptions that inclinations have a uniform distribution on the sphere.

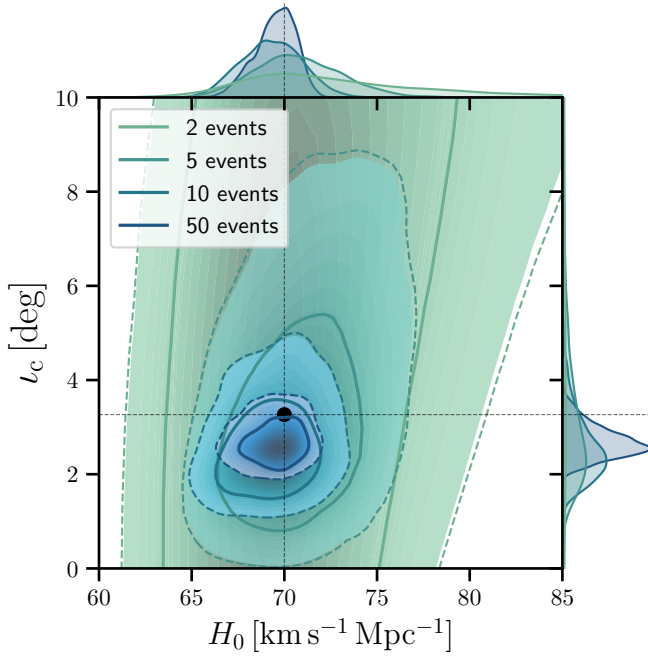


Fig. 3. Joint constraint on H_0 and the half-width of the jet ι_c . Dashed (solid) lines indicate the 95% (68%) C.L..

population prior and the EM detection probability. Remarkably, an accurate measurements of the viewing angle $\Theta_i = \min\{\iota_i, 180^\circ - \iota_i\}$ for each event is obtained just from the deconvolution of the latter, even in absence of a direct measurement of this angle in the EM (see [28] for a similar approach). These unbiased measurements are shown in Fig. 4 as a function of redshift for the case of 10 events as green dots,⁴ and recover the injected values (black stars) within $\sim 1\sigma$ with good accuracy. The inferred values are below the reconstructed maximum viewing angle Θ_{\max} at any redshift (green band). In contrast, the measurement from GW data only (blue points) is largely inaccurate, as expected (see Fig. 1).

Finally, to provide an idea of the information that we can extract with this technique from the only event with counterpart detected so far, and to show that our pipeline can be straightforwardly applied to actual detections, the violin plot in yellow in Fig. 4 shows the result obtained with the analysis of GW170817 and its counterpart, assuming a Gaussian shaped profile for the jet.⁵

Conclusions and discussion. The bias arising from EM

⁴We find that 50 events at O5 sensitivity give only a marginal improvement due to the small horizon of the GW detectors.

⁵We use the “high spin” posterior samples available on GWOSC [61], the redshift given in [62] and compute the detection probability with an injection set generated with O2 sensitivity and an optimal SNR cut $\rho_{\text{opt}} \geq 10$ [63]. We find that the posterior probability on H_0 is perfectly compatible with the result of [62] even when including the EM detection probability, as expected with a sample of 1 event only and in line with the results of our simulations.

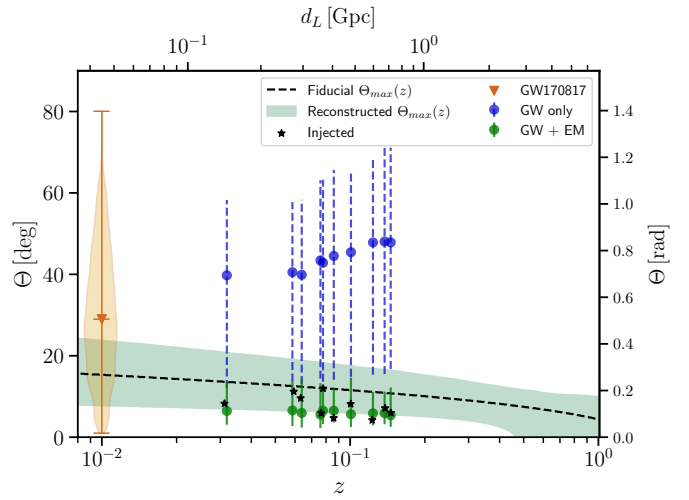


Fig. 4. Reconstruction of the maximum inclination angle of the GRB as a function of redshift from 10 simulated multimessenger events. The fiducial model is shown as a black, dashed line. Dots with errorbars indicate the measurements without (blue) and with (green) the inclusion of the EM detection probability. Black stars denote the injected values. The yellow violin plot shows, for comparison, the result for the viewing angle of GW170817 obtained with the method proposed in this work.

selection effects can be a major limitation for standard siren cosmology already in the short term. In this work, we provided a new method to properly deconvolve it. We can summarize the main novelties as follows:

- *Unbiased inference of H_0 in the short term.* It is possible to accurately measure H_0 by inferring the EM detection probability from multimessenger data only, and without the need of modeling explicitly the GRB detector, starting from as few as two sources, which could become a concrete scenario in the near future. In this case, the inference scheme introduced here would be directly applicable, demonstrated by applying our pipeline to GW170817.
- *Determination of the GRB emission profile and individual viewing angles.* The proposed inference scheme leads to a reconstruction of the GRB emission profile as well as to an accurate and precise measurement of the inclination of each event. The same can be used in conjunction with a prior on H_0 (from either CMB or SNe) to determine the GRB structure only from GW data and redshift measurements (see [29, 64, 65]).

These results open other possibilities:

- *More accurate modeling of the EM emission.* More general models of the EM selection function can be straightforwardly included, such as a limited redshift range for the EM detections, a dependence of the EM emission on the masses, a selection of

GW sources based on their sky localization, and the Field of View of the EM instrument. We plan to address these aspects in future work.

- *Model-independent approaches.* In this work, for simplicity, the functional dependence of the flux from inclination used for inference was the same used to generate the EM data. Importantly, this assumption can be relaxed and is not essential to the method. One can adopt a more agnostic approach and model the EM detection probability as a flexible function (e.g. a polynomial or a Gaussian process) to be less prone to modeling systematics. On the other hand, using physically motivated models can be of interest for determining if different emission mechanisms provide a better fit to the data, e.g. by comparing the respective Bayes factors [64, 65].
- *Independent inclination measurements.* We assumed that independent inclination measurements (e.g. from VLBI) are not present to stress the generality of the method. Nonetheless, such measurements can be straightforwardly included by adding the corresponding likelihood in Eq. (1). In this case, however, additional sources of bias might be present, as shown in [16].
- *Population properties and perspectives for 3G detectors.* GW and EM observatories of next generation are under active development [66–68]. Besides H_0 , our inference scheme includes the reconstruction of the mass and redshift distributions of the BNS population, as well as the full distance–redshift relation, including the matter energy density and the Dark

Energy Equation of State. It can also be straightforwardly extended to test the effect of modified GW propagation [69, 70]. With 3G sensitivities, we will be able to precisely determine all those. We will provide forecasts in future work.

With more multimessenger events in the near future and major new experiments planned, we hope that this work will contribute to advancing towards accurate and precise standard siren cosmology both in the short and long term.

Acknowledgments. We thank Simone Mastrogiovanni for LVK internal review; Om Salafia, Matthew Mould, Davide Gerosa, Hsin-Yu Chen for useful comments on the draft; Marica Branchesi and Samuele Ronchini for useful exchanges in the initial stage of the work; Massimo Dotti, Costantino Pacilio, Arianna Renzini, Pippa Cole, and Alberto Colombo for discussions. `gwfast` is publicly available at github.com/cosmostatgw/gwfast. `PyMC` is available at pymc.io. M.Manc. is supported by European Union’s H2020 ERC Starting Grant No. 945155–GWmining and Cariplo Foundation Grant No. 2021-0555. The work of M.Manc. received support from the French government under the France 2030 investment plan, as part of the Initiative d’Excellence d’Aix-Marseille Université – A*MIDEX AMX-22-CEI-02. F.I, S.F., M.Mag and N.M. are supported by the Swiss National Science Foundation, grant 200020_191957, and by the SwissMap National Center for Competence in Research. This work made use of the clusters Yggdrasil and Baobab at the University of Geneva. This document has LIGO DCC number LIGO-P2400167.

-
- [1] M. Moresco, L. Amati, L. Amendola, *et al.*, *Living Rev. Rel.* **25**, 6 (2022), [arXiv:2201.07241](https://arxiv.org/abs/2201.07241) [astro-ph.CO].
 - [2] B. F. Schutz, *Nature* **323**, 310 (1986).
 - [3] B. P. Abbott, R. Abbott, T. D. Abbott, *et al.* (LIGO Scientific, Virgo), *Phys. Rev. Lett.* **119**, 161101 (2017), [arXiv:1710.05832](https://arxiv.org/abs/1710.05832) [gr-qc].
 - [4] B. P. Abbott, R. Abbott, T. D. Abbott, *et al.* (LIGO Scientific, Virgo, Fermi GBM, INTEGRAL, IceCube, AstroSat Cadmium Zinc Telluride Imager Team, IPN, Insight-Hxmt, ANTARES, Swift, AGILE Team, 1M2H Team, Dark Energy Camera GW-EM, DES, DLT40, GRAWITA, Fermi-LAT, ATCA, ASKAP, Las Cumbres Observatory Group, OzGrav, DWF (Deeper Wider Faster Program), AST3, CAASTRO, VINROUGE, MASTER, J-GEM, GROWTH, JAGWAR, CaltechNRAO, TTU-NRAO, NuSTAR, Pan-STARRS, MAXI Team, TZAC Consortium, KU, Nordic Optical Telescope, ePESSTO, GROND, Texas Tech University, SALT Group, TOROS, BOOTES, MWA, CALET, IKI-GW Follow-up, H.E.S.S., LOFAR, LWA, HAWC, Pierre Auger, ALMA, Euro VLBI Team, Pi of Sky, Chandra Team at McGill University, DFN, ATLAS Telescopes, High Time Resolution Universe Survey, RI-MAS, RATIR, SKA South Africa/MeerKAT), *Astrophys. J. Lett.* **848**, L12 (2017), [arXiv:1710.05833](https://arxiv.org/abs/1710.05833) [astro-ph.HE].
 - [5] B. P. Abbott, R. Abbott, T. Abbott, *et al.* (LIGO Scientific, Virgo), *Phys. Rev. X* **9**, 011001 (2019), [arXiv:1805.11579](https://arxiv.org/abs/1805.11579) [gr-qc].
 - [6] S. Nissanke, D. E. Holz, N. Dalal, S. A. Hughes, J. L. Sievers, and C. M. Hirata, (2013), [arXiv:1307.2638](https://arxiv.org/abs/1307.2638) [astro-ph.CO].
 - [7] H.-Y. Chen, M. Fishbach, and D. E. Holz, *Nature* **562**, 545 (2018), [arXiv:1712.06531](https://arxiv.org/abs/1712.06531) [astro-ph.CO].
 - [8] S. M. Feeney, H. V. Peiris, A. R. Williamson, S. M. Nissanke, D. J. Mortlock, J. Alsing, and D. Scolnic, *Phys. Rev. Lett.* **122**, 061105 (2019), [arXiv:1802.03404](https://arxiv.org/abs/1802.03404) [astro-ph.CO].
 - [9] A. G. Riess, W. Yuan, L. M. Macri, *et al.*, *Astrophys. J. Lett.* **934**, L7 (2022), [arXiv:2112.04510](https://arxiv.org/abs/2112.04510) [astro-ph.CO].
 - [10] N. Aghanim, Y. Akrami, F. Arroja, *et al.* (Planck), *Astron. Astrophys.* **641**, A1 (2020), [arXiv:1807.06205](https://arxiv.org/abs/1807.06205) [astro-ph.CO].
 - [11] S. Mozzon, G. Ashton, L. K. Nuttall, and A. R. Williamson, *Phys. Rev. D* **106**, 043504 (2022), [arXiv:2110.11731](https://arxiv.org/abs/2110.11731) [astro-ph.CO].

- [12] Y. Huang, H.-Y. Chen, C.-J. Haster, L. Sun, S. Vitale, and J. Kissel, (2022), [arXiv:2204.03614 \[gr-qc\]](#).
- [13] C. Nicolaou, O. Lahav, P. Lemos, W. Hartley, and J. Braden, *Mon. Not. Roy. Astron. Soc.* **495**, 90 (2020), [arXiv:1909.09609 \[astro-ph.CO\]](#).
- [14] C. Howlett and T. M. Davis, *Mon. Not. Roy. Astron. Soc.* **492**, 3803 (2020), [arXiv:1909.00587 \[astro-ph.CO\]](#).
- [15] S. Mukherjee, G. Lavaux, F. R. Bouchet, J. Jasche, B. D. Wandelt, S. M. Nissanke, F. Leclercq, and K. Hotokezaka, *Astron. Astrophys.* **646**, A65 (2021), [arXiv:1909.08627 \[astro-ph.CO\]](#).
- [16] H.-Y. Chen, *Phys. Rev. Lett.* **125**, 201301 (2020), [arXiv:2006.02779 \[astro-ph.HE\]](#).
- [17] K. Mooley, A. Deller, O. Gottlieb, E. Nakar, G. Hallinan, S. Bourke, D. Frail, A. Horesh, A. Corsi, and K. Hotokezaka, *Nature* **561**, 355 (2018), [arXiv:1806.09693 \[astro-ph.HE\]](#).
- [18] K. Hotokezaka, E. Nakar, O. Gottlieb, S. Nissanke, K. Masuda, G. Hallinan, K. P. Mooley, and A. Deller, *Nature Astron.* **3**, 940 (2019), [arXiv:1806.10596 \[astro-ph.CO\]](#).
- [19] G. Gianfagna, L. Piro, F. Pannarale, H. Van Eerten, F. Ricci, and G. Ryan, *Mon. Not. Roy. Astron. Soc.* **528**, 2600 (2024), [arXiv:2309.17073 \[astro-ph.HE\]](#).
- [20] G. Gianfagna, L. Piro, F. Pannarale, H. Van Eerten, F. Ricci, G. Ryan, and E. Troja, *Mon. Not. Roy. Astron. Soc.* **523**, 4771 (2023), [arXiv:2212.01104 \[astro-ph.HE\]](#).
- [21] S. Mastroianni, R. Duque, E. Chassande-Mottin, F. Daigne, and R. Mochkovitch, *Astron. Astrophys.* **652**, A1 (2021), [arXiv:2012.12836 \[astro-ph.HE\]](#).
- [22] H.-Y. Chen, C. Talbot, and E. A. Chase, (2023), [arXiv:2307.10402 \[astro-ph.CO\]](#).
- [23] S. Gagnon-Hartman, J. Ruan, and D. Haggard, *Mon. Not. Roy. Astron. Soc.* **520**, 1 (2023), [arXiv:2301.05241 \[astro-ph.CO\]](#).
- [24] A. Colombo, O. S. Salafia, F. Gabrielli, G. Ghirlanda, B. Giacomazzo, A. Perego, and M. Colpi, *Astrophys. J.* **937**, 79 (2022), [arXiv:2204.07592 \[astro-ph.HE\]](#).
- [25] T. J. Loredo, *AIP Conf. Proc.* **735**, 195 (2004), [arXiv:astro-ph/0409387](#).
- [26] I. Mandel, W. M. Farr, and J. R. Gair, *Mon. Not. Roy. Astron. Soc.* **486**, 1086 (2019), [arXiv:1809.02063 \[physics.data-an\]](#).
- [27] S. Vitale, D. Gerosa, W. M. Farr, and S. R. Taylor, in *Handbook of Gravitational Wave Astronomy* (Springer, Singapore, 2022) p. 45, [arXiv:2007.05579 \[astro-ph.IM\]](#).
- [28] A. Farah, R. Essick, Z. Doctor, M. Fishbach, and D. E. Holz, *Astrophys. J.* **895**, 108 (2020), [arXiv:1912.04906 \[astro-ph.HE\]](#).
- [29] O. S. Salafia, M. E. Rasio, G. Ghirlanda, and I. Mandel, *Astron. Astrophys.* **680**, A45 (2023), [arXiv:2306.15488 \[astro-ph.HE\]](#).
- [30] M. Mould, C. J. Moore, and D. Gerosa, *Phys. Rev. D* **109**, 063013 (2024), [arXiv:2311.12117 \[gr-qc\]](#).
- [31] R. Essick and M. Fishbach, *Astrophys. J.* **962**, 169 (2024), [arXiv:2310.02017 \[gr-qc\]](#).
- [32] M. Vallisneri, *Phys. Rev. D* **77**, 042001 (2008), [arXiv:gr-qc/0703086](#).
- [33] F. Iacovelli, M. Mancarella, S. Foffa, and M. Maggiore, *Astrophys. J.* **941**, 208 (2022), [arXiv:2207.02771 \[gr-qc\]](#).
- [34] U. Dupletsa, J. Harms, K. K. Y. Ng, J. Tisino, F. Santoliquido, and A. Cozzumbo, (2024), [arXiv:2404.16103 \[gr-qc\]](#).
- [35] U. Dupletsa, J. Harms, B. Banerjee, M. Branchesi, B. Goncharov, A. Maselli, A. C. S. Oliveira, S. Ronchini, and J. Tisino, *Astron. Comput.* **42**, 100671 (2023), [arXiv:2205.02499 \[gr-qc\]](#).
- [36] H.-Y. Chen, S. Vitale, and R. Narayan, *Phys. Rev. X* **9**, 031028 (2019), [arXiv:1807.05226 \[astro-ph.HE\]](#).
- [37] E. Chassande-Mottin, K. Leyde, S. Mastroianni, and D. A. Steer, *Phys. Rev. D* **100**, 083514 (2019), [arXiv:1906.02670 \[astro-ph.CO\]](#).
- [38] J. M. S. de Souza and R. Sturani, *Phys. Rev. D* **108**, 043027 (2023), [arXiv:2302.07749 \[gr-qc\]](#).
- [39] M. Li, J. Yu, and Z. Pan, (2024), [arXiv:2403.01846 \[gr-qc\]](#).
- [40] S. Borhanian, *Class. Quant. Grav.* **38**, 175014 (2021), [arXiv:2010.15202 \[gr-qc\]](#).
- [41] F. Iacovelli, M. Mancarella, S. Foffa, and M. Maggiore, *Astrophys. J. Suppl.* **263**, 2 (2022), [arXiv:2207.06910 \[astro-ph.IM\]](#).
- [42] G. Ashton, M. Hübner, P. D. Lasky, C. Talbot, *et al.*, *Astrophys. J. Suppl.* **241**, 27 (2019), [arXiv:1811.02042 \[astro-ph.IM\]](#).
- [43] R. J. E. Smith, G. Ashton, A. Vajpeyi, and C. Talbot, *Mon. Not. Roy. Astron. Soc.* **498**, 4492 (2020), [arXiv:1909.11873 \[gr-qc\]](#).
- [44] A. H. Nitz and T. Dal Canton, *Astrophys. J. Lett.* **917**, L27 (2021), [arXiv:2106.15259 \[astro-ph.HE\]](#).
- [45] R. Smith, S. Borhanian, B. Sathyaprakash, *et al.*, *Phys. Rev. Lett.* **127**, 081102 (2021), [arXiv:2103.12274 \[gr-qc\]](#).
- [46] K. W. K. Wong, M. Isi, and T. D. P. Edwards, *Astrophys. J.* **958**, 129 (2023), [arXiv:2302.05333 \[astro-ph.IM\]](#).
- [47] T. Wouters, P. T. H. Pang, T. Dietrich, and C. Van Den Broeck, (2024), [arXiv:2404.11397 \[astro-ph.IM\]](#).
- [48] S. Ronchini, M. Branchesi, G. Oganesyan, B. Banerjee, U. Dupletsa, G. Ghirlanda, J. Harms, M. Mapelli, and F. Santoliquido, *Astron. Astrophys.* **665**, A97 (2022), [arXiv:2204.01746 \[astro-ph.HE\]](#).
- [49] J. Aasi, B. P. Abbott, R. Abbott, *et al.* (LIGO Scientific), *Class. Quant. Grav.* **32**, 074001 (2015), [arXiv:1411.4547 \[gr-qc\]](#).
- [50] F. Acernese, M. Agathos, K. Agatsuma, *et al.* (Virgo), *Class. Quant. Grav.* **32**, 024001 (2015), [arXiv:1408.3978 \[gr-qc\]](#).
- [51] Y. Aso, Y. Michimura, K. Somiya, M. Ando, O. Miyakawa, T. Sekiguchi, D. Tatsumi, and H. Yamamoto (KAGRA), *Phys. Rev. D* **88**, 043007 (2013), [arXiv:1306.6747 \[gr-qc\]](#).
- [52] LIGO-India, Proposal of the Consortium for Indian Initiative in Gravitational-wave Observations, <https://dcc.ligo.org/LIGO-M1100296/public> (2011).
- [53] B. P. Abbott, R. Abbott, T. D. Abbott, *et al.* (KAGRA, LIGO Scientific, Virgo), *Living Rev. Rel.* **23**, 3 (2020), [arXiv:1304.0670 \[gr-qc\]](#).
- [54] C. Meegan, G. Lichti, P. N. Bhat, *et al.*, *Astrophys. J.* **702**, 791 (2009), [arXiv:0908.0450 \[astro-ph.IM\]](#).
- [55] P. Madau and M. Dickinson, *Ann. Rev. Astron. Astrophys.* **52**, 415 (2014), [arXiv:1403.0007 \[astro-ph.CO\]](#).
- [56] E. Troja, L. Piro, G. Ryan, H. van Eerten, R. Ricci, M. Wieringa, S. Lotti, T. Sakamoto, and S. B. Cenko, *Mon. Not. Roy. Astron. Soc.* **478**, L18 (2018), [arXiv:1801.06516 \[astro-ph.HE\]](#).
- [57] O. Abril-Pla, V. Andreani, C. Carroll, L. Dong, C. J. Farnesbeck, M. Kochurov, R. Kumar, J. Lao, C. C. Luhmann, O. A. Martin, M. Osthege, R. Vieira, T. V. Wiecki, and R. Zinkov, *PeerJ Computer Science* **9**, e1516 (2023).
- [58] S. Brooks, A. Gelman, G. Jones, and X.-L. Meng, *Handbook of Markov Chain Monte Carlo* (Chapman and Hall/CRC, 2011).

- [59] M. D. Hoffman and A. Gelman, *Journal of Machine Learning Research* **15**, 1593 (2014), arXiv:1111.4246 [stat.CO].
- [60] A. Colombo, O. S. Salafia, F. Gabrielli, G. Ghirlanda, B. Giacomazzo, A. Perego, and M. Colpi, *Astrophys. J.* **937**, 79 (2022), arXiv:2204.07592 [astro-ph.HE].
- [61] R. Abbott, T. D. Abbott, S. Abraham, *et al.* (LIGO Scientific, Virgo), *SoftwareX* **13**, 100658 (2021), arXiv:1912.11716 [gr-qc].
- [62] B. P. Abbott, R. Abbott, T. D. Abbott, *et al.* (LIGO Scientific, Virgo, 1M2H, Dark Energy Camera GW-E, DES, DLT40, Las Cumbres Observatory, VINROUGE, MASTER), *Nature* **551**, 85 (2017), arXiv:1710.05835 [astro-ph.CO].
- [63] R. Abbott, T. D. Abbott, F. Acernese, *et al.* (KAGRA, Virgo, LIGO Scientific), *Phys. Rev. X* **13**, 011048 (2023), arXiv:2111.03634 [astro-ph.HE].
- [64] F. Hayes, I. S. Heng, J. Veitch, and D. Williams, *Astrophys. J.* **891**, 124 (2020), arXiv:1911.04190 [astro-ph.HE].
- [65] F. Hayes, I. S. Heng, G. Lamb, E.-T. Lin, J. Veitch, and M. J. Williams, *Astrophys. J.* **954**, 92 (2023), arXiv:2305.06275 [astro-ph.HE].
- [66] M. Maggiore, C. Van Den Broeck, N. Bartolo, *et al.*, *JCAP* **2020** (03), 050, arXiv:1912.02622 [astro-ph.CO].
- [67] M. Evans, R. X. Adhikari, C. Afle, *et al.*, (2021), arXiv:2109.09882 [astro-ph.IM].
- [68] M. Branchesi, M. Maggiore, D. Alonso, *et al.*, *JCAP* **2023** (07), 068, arXiv:2303.15923 [gr-qc].
- [69] E. Belgacem, Y. Dirian, S. Foffa, and M. Maggiore, *Phys. Rev. D* **97**, 104066 (2018), arXiv:1712.08108 [astro-ph.CO].
- [70] E. Belgacem, Y. Dirian, S. Foffa, and M. Maggiore, *Phys. Rev. D* **98**, 023510 (2018), arXiv:1805.08731 [gr-qc].
- [71] A. Finke, S. Foffa, F. Iacovelli, M. Maggiore, and M. Mancarella, *JCAP* **2021** (08), 026, arXiv:2101.12660 [astro-ph.CO].
- [72] M. Maggiore, *Gravitational Waves. Vol. 1: Theory and Experiments*, Oxford Master Series in Physics (Oxford University Press, 2007).
- [73] M. Kole, F. Iacovelli, M. Mancarella, and N. Produit, *Astron. Astrophys.* **669**, A77 (2023), arXiv:2211.12403 [astro-ph.HE].
- [74] N. Farrow, X.-J. Zhu, and E. Thrane, *Astrophys. J.* **876**, 18 (2019), arXiv:1902.03300 [astro-ph.HE].
- [75] J. Yu, H. Song, S. Ai, H. Gao, F. Wang, Y. Wang, Y. Lu, W. Fang, and W. Zhao, *Astrophys. J.* **916**, 54 (2021), arXiv:2104.12374 [astro-ph.HE].
- [76] B. Zhang, X.-Y. Dai, N. M. Lloyd-Ronning, and P. Meszaros, *Astrophys. J. Lett.* **601**, L119 (2004), arXiv:astro-ph/0311190.
- [77] E. J. Howell, K. Ackley, A. Rowlinson, and D. Coward, *Monthly Notices of the Royal Astronomical Society* **485**, 1435 (2019), arXiv:1811.09168 [astro-ph.HE].
- [78] E. Belgacem, Y. Dirian, S. Foffa, E. J. Howell, M. Maggiore, and T. Regimbau, *JCAP* **2019** (08), 015, arXiv:1907.01487 [astro-ph.CO].
- [79] M. Karamanis, F. Beutler, and J. A. Peacock, *Mon. Not. Roy. Astron. Soc.* **508**, 3589 (2021), arXiv:2105.03468 [astro-ph.IM].
- [80] M. Karamanis and F. Beutler, *Stat. Comput.* **31**, 61 (2021), arXiv:2002.06212 [stat.ML].
- [81] V. Tiwari, *Class. Quant. Grav.* **35**, 145009 (2018), arXiv:1712.00482 [astro-ph.HE].
- [82] W. M. Farr, M. Fishbach, J. Ye, and D. Holz, *Astrophys. J. Lett.* **883**, L42 (2019), arXiv:1908.09084 [astro-ph.CO].

- [83] F. Pedregosa, G. Varoquaux, A. Gramfort, V. Michel, B. Thirion, O. Grisel, M. Blondel, P. Prettenhofer, R. Weiss, V. Dubourg, *et al.*, *J. Mach. Learn. Res.* **12**, 2825 (2011), arXiv:1201.0490 [cs.LG].

Appendix A: Derivation of the hierarchical posterior

We consider a set of events with single-event parameters $\{\theta_i\}_{i=1}^{N_{\text{obs}}}$ and data $\{\mathcal{D}\}_{i=1}^{N_{\text{obs}}}$. We also introduce a set of boolean variables $\{\text{det}_i\}_{i=1}^{N_{\text{obs}}}$ where $\text{det}_i = 1$ if the event is detected and 0 otherwise. As common in GW population studies, the hierarchical model is an inhomogeneous Poisson process [25, 26]. The expected number of sources is defined as $N_{\text{exp}}(\lambda) = N P(\text{det}|\lambda)$ with

$$P(\text{det}|\lambda) = \int d\theta d\mathcal{D} p_{\text{pop}}(\theta|\lambda) \mathcal{L}(\mathcal{D}|\theta) P(\text{det}|\mathcal{D}, \theta, \lambda). \quad (\text{A1})$$

In the literature, $P(\text{det}|\lambda)$ is often denoted as $\alpha(\lambda)$,⁶ and represents the fraction of detectable events given hyperparameters λ , while usually the integral $\int d\mathcal{D} \mathcal{L}(\mathcal{D}|\theta) P(\text{det}|\mathcal{D}, \theta, \lambda) = \int_{f(\mathcal{D}) \geq 0} d\mathcal{D} \mathcal{L}(\mathcal{D}|\theta)$ is denoted as $P_{\text{det}}(\theta)$ [or more correctly $\bar{P}(\text{det}|\theta)$], under the assumption that $P(\text{det}_i|\mathcal{D}, \theta, \lambda) = P(\text{det}|\mathcal{D})$ and that $P(\text{det}|\mathcal{D})$ is an indicator function equal to 1 if $f(\mathcal{D}) \geq 0$ and 0 otherwise, see below. Concretely, in GW population studies one often assumes $f(\mathcal{D}) = \rho_{\text{obs}} - \rho_{\text{th}}$ where ρ_{obs} is the observed SNR in the detector and ρ_{th} a given threshold that defines a detection.

Including explicitly the variables $\{\text{det}_i\}_{i=1}^{N_{\text{obs}}}$, the hierarchical likelihood can be written as [26, 31]

$$p(\{\theta_i\}, \{\mathcal{D}_i\}, \{\text{det}_i\}|\lambda) = N^{N_{\text{obs}}} e^{-NP(\text{det}|\lambda)} \times \prod_{i=1}^{N_{\text{obs}}} p(\text{det}_i, \mathcal{D}_i, \theta_i|\lambda), \quad (\text{A2})$$

where in full generality

$$\begin{aligned} p(\text{det}_i, \mathcal{D}_i, \theta_i|\lambda) &= \mathcal{L}(\text{det}_i, \mathcal{D}_i|\theta_i) p_{\text{pop}}(\theta_i|\lambda) \\ &= P(\text{det}_i|\mathcal{D}_i, \theta_i, \lambda) \mathcal{L}(\mathcal{D}_i|\theta_i) p_{\text{pop}}(\theta_i|\lambda). \end{aligned} \quad (\text{A3})$$

At this point, the usual assumption in GW astronomy is that detectability is a function of the data only, and not of the (true, unknown) source parameters θ_i , nor of the hyperparameters λ . This implies $P(\text{det}_i|\mathcal{D}_i, \theta_i, \lambda) = P(\text{det}_i|\mathcal{D}_i)$. Finally, assuming that detection is a deterministic function of the data, one has $P(\text{det}_i|\mathcal{D}_i) = 1 \forall i$ since each event in the catalog has obviously been detected.⁷ This is what we assume for GW data also in this

⁶The notation $\beta(\lambda)$ or $\sigma(\lambda)$ is also adopted.

⁷It can be shown that the likelihood is independent of this term even in the more general case in which the detection is a probabilistic function of the data provided that it is independent of the true source parameters θ_i [31].

work – an event is detected if the *observed* SNR exceeds a given threshold.

However, we might be in a situation where detectability depends on some (unknown) source parameters that are not measured by the experiment. In this case, we have no data available for all the parameters determining detectability, but we know that a detection happened, and we can include this information. In particular, we assume that detectability has an a-priori unknown dependence on some of the (equally unknown) source parameters θ_i through a subset of hyperparameters $\tilde{\lambda}$ that we wish to determine from data. In this case, $P(\text{det}_i|\mathcal{D}_i, \theta_i, \tilde{\lambda})$ is not equal to one for all θ_i . This term will appear in the likelihood and the parameters $\tilde{\lambda}$ can be determined from the data. This is the case for the EM data in this work, as we now detail.

Turning to the specific case of interest for this paper, we assume that the likelihood is composed by GW and EM data with independent noise, $\mathcal{L}(\mathcal{D}|\theta, z) = \mathcal{L}(\mathcal{D}_{\text{GW}}|\theta) \mathcal{L}(z_{\text{EM}}^{\text{obs}}|z)$. We denote by $\{\mathcal{D}_{\text{GW}}^i, \mathcal{D}_{\text{EM}}^i\}_{i=1}^{N_{\text{obs}}}$ the two datasets, with $\mathcal{D}_{\text{EM}} = \{z_{\text{EM}}^{\text{obs}}\}$. The parameters θ refer to detector-frame parameters of the GW waveform while z denotes the true redshift. The GW likelihood is discussed in App. B. As anticipated, the GW measurement is modeled as a deterministic function of the data.

Turning to the EM sector, crucially, in this work we assume that we are not able to obtain a measurement of all the variables determining the EM detections. Explicitly, for the problem under consideration in this paper, the EM data consist only in a redshift measurement, following from the identification of the host galaxy from the GRB emission.⁸ We expect that the detection of the source can happen only under certain conditions on its inclination (namely, the inclination has to be small enough in order to observe a relativistic jet), but we remain agnostic about the data from the GRB observatory (see [29] for an explicit modeling), and assume that we are just given an observed redshift $z_{\text{EM}}^{\text{obs}}$ (for which we will assume a Gaussian likelihood with standard deviation σ_z).

We then assume that the EM detection has a dependence on the source parameters and the hyperparameters λ_{EM} describing the GRB jet structure. Hence, $P(\text{det}_i|\mathcal{D}_i, \theta_i, \tilde{\lambda}) = P(\text{det}_{\text{GW}}|\mathcal{D}_{\text{GW}})P(\text{det}_{\text{EM}}|\theta, \lambda_{\text{EM}}) = P(\text{det}_{\text{EM}}|\theta, \lambda_{\text{EM}})$.

Finally, the population prior is

$$p_{\text{pop}}(\theta|\lambda) \propto \frac{\psi(z, \lambda_z)}{1+z} \frac{dV_c}{dz} \frac{p(m_1, m_2|\lambda_m)}{\frac{\partial d_L}{\partial z}(z, \lambda_c) (1+z)^2} \bigg|_{\substack{m_i = \frac{m_i^{\text{det}}}{1+z(d_L, \lambda_c)} \\ z = z(d_L, \lambda_c)}}, \quad (\text{A4})$$

⁸Notice that, even if we assume an EM likelihood for the redshift only, crucially the counterpart detection provides also a very accurate measurement of the sky position of the source and of the GPS time of the event. This information in our setting is already incorporated in the GW likelihood, which we compute keeping these parameters fixed.

where $p(m_1, m_2|\lambda_m)$ is the source-frame mass distribution with hyperparameters λ_m , $\psi(z, \lambda_z)$ is the source-frame merger rate distribution with hyperparameters λ_z , dV_c/dz is the differential comoving volume, the factor $1/(1+z)$ takes into account time dilation from source to detector frame, and the factor $(1+z)^2 \partial d_L / \partial z(z, \lambda_c)$ at the denominator comes from conversion of the prior from detector- to source-frame variables. Explicitly, the distance-redshift relation in a flat Λ CDM Universe is given by

$$d_L(z, \lambda_c) = \frac{c(1+z)}{H_0} \int_0^z \frac{dz'}{\sqrt{\Omega_{m,0}(1+z')^3 + 1 - \Omega_{m,0}}}. \quad (\text{A5})$$

The cosmological hyperparameters are denoted by $\lambda_c = \{H_0, \Omega_{m,0}\}$. The full set of hyperparameters is defined by $\lambda = \{\lambda_c, \lambda_m, \lambda_z, \lambda_{\text{EM}}\}$.

We will work in detector-frame; hence, in Eq. (A4) the source-frame quantities are computed from the detector-frame ones with a dependence on the cosmology. In particular, the redshift can always be re-expressed as a function of the luminosity distance and of the cosmological parameters λ_c [71]; we will assume to have performed this change of variables and denote the EM likelihood as $\mathcal{L}(\mathcal{D}_{\text{EM}}^i|\theta_i, \lambda_c) = \mathcal{L}(z_{\text{EM},i}^{\text{obs}}|z(d_{L,i}, \lambda_c))$.

Putting everything together in Eq. (A2), adding a prior $\pi(\lambda)$ on the hyperparameters, and marginalizing over the overall number of expected events N with a prior $\propto 1/N$ [26], we arrive at the hierarchical likelihood in Eq. (1).

Interestingly, we can also make an explicit link to the modeling of the likelihood of the GRB experiment [29].⁹ In this case, one would observe a flux with the observation described by a likelihood of the form $\mathcal{L}(F_i^{\text{obs}}|F_i)$. Each term in the product at the numerator of Eq. (1) would then be of the form

$$\mathcal{L}(\mathcal{D}_{\text{GW}}^i|\theta_i) \mathcal{L}(z_{\text{EM},i}^{\text{obs}}|z(d_{L,i}, \lambda_c)) \mathcal{L}(F_i^{\text{obs}}|F_i) \times p_{\text{pop}}(\theta_i|\lambda) p_{\text{pop}}(F|\theta_i, \lambda_{\text{jet}}), \quad (\text{A6})$$

where λ_{jet} are the parameters describing the GRB jet structure (e.g. $\{A_0, \iota_c\}$ in this paper). Being agnostic on the GRB data is equivalent to marginalize the likelihood over the observed flux F_i^{obs} , which gives for each event a contribution

$$\int dF_i^{\text{obs}} \mathcal{L}(F_i^{\text{obs}}|F_i) p_{\text{pop}}(F_i|\theta_i, \lambda_{\text{jet}}). \quad (\text{A7})$$

The population prior on the flux is given by the relation between the latter and the source parameters determining its shape, $p_{\text{pop}}(F|\theta_i, \lambda) = \delta(F - F(\theta_i, \lambda_{\text{jet}}))$, so F can be integrated out of the likelihood (see e.g. Eq. (C1) below for the model of $F(\theta_i, \lambda_{\text{jet}})$ used in this work). Moreover, the integral in Eq. (A7) can be restricted

⁹We are grateful to Om Salafia for discussions on this point.

to the domain of observable EM data (i.e. those with $F_i^{\text{obs}} > F_{\text{th}}$ for a given detection threshold F_{th}) by writing $\mathcal{L}(F_i^{\text{obs}}|F_i) = \mathcal{L}(\det_{\text{EM},i}, F_i^{\text{obs}}|F_i) + \mathcal{L}(\neg\det_{\text{EM},i}, F_i^{\text{obs}}|F_i)$ where $\neg\det_{\text{EM},i}$ denotes a non-detection. By definition, the second term is zero while the first is $\mathcal{L}(\det_{\text{EM},i}, F_i^{\text{obs}}|F_i) = P(\det_{\text{EM},i}|F_i^{\text{obs}})\mathcal{L}(F_i^{\text{obs}}|F_i) = \mathcal{L}(F_i^{\text{obs}}|F_i)$ because for detected events $P(\det_{\text{EM},i}|F_i^{\text{obs}}) = 1$. So, Eq. (A7) becomes

$$\int_{F_i^{\text{obs}} \geq F_{\text{th}}} dF_i^{\text{obs}} \mathcal{L}(F_i^{\text{obs}}|F(\theta_i, \lambda_{\text{jet}})) \equiv P(\det_{\text{EM}}^i|\theta_i, \lambda_{\text{EM}}), \quad (\text{A8})$$

which leads again to Eq. (1), and we defined $\lambda_{\text{EM}} = \{A_0, \iota_c, F_{\text{th}}\}$.

Appendix B: Extended likelihood approximant

1. Effects of detector noise

We start by discussing the inclusion of the effects of detector noise in the simulation. The GW likelihood is

$$-2 \log \mathcal{L}(\mathcal{D}_{\text{GW}} | \theta) \propto (\mathcal{D}_{\text{GW}} - h(\theta) | \mathcal{D}_{\text{GW}} - h(\theta)), \quad (\text{B1})$$

with $\mathcal{D}_{\text{GW}} = h_0 + n$ denoting the signal, $h_0 = h(\theta_0)$ the waveform evaluated at the true parameters θ_0 , and n the noise. The notation $(\cdot|\cdot)$ indicates the inner product in the frequency domain [72], $(a|b) = 4\text{Re} \int_0^\infty \tilde{a}^*(f)\tilde{b}(f)/S_n(f)$, with $S_n(f)$ the noise one-sided power spectral density (PSD), defined by $\langle \tilde{n}^*(f)\tilde{n}(f') \rangle = \delta(f - f')S_n(f)/2$. The usual FIM approximation consists in expanding the likelihood at linear order around the point h_0 , i.e. $h(\theta) \approx h_0 + h_i \delta\theta^i$ (with $h_i \equiv \partial_{\theta_i} h|_{\theta_0}$ and $\delta\theta^i = \theta^i - \theta_0^i$), obtaining¹⁰

$$-2 \log \mathcal{L}(\mathcal{D}_{\text{GW}} | \theta) \propto \delta\theta^i \delta\theta^j (h_i | h_j) - 2\delta\theta^i (n | h_i). \quad (\text{B2})$$

The covariance $(h_i | h_j)^{-1}$ obtained this way does not encode the effect of noise fluctuations, as it is computed at the point h_0 . This is not fully consistent with the selection cut applied to obtain the GW catalog, which, as discussed previously, should depend only on the observed data, including noise fluctuations [31].¹¹

We include the effect of detector noise as follows. We restrict for clarity to the case of the FIM, neglecting higher-order corrections, but the argument does not depend on this assumption. For each simulated event with true parameters θ_0 , and for each GW detector in the network under consideration, we generate an explicit realization of the noise from the PSD in the frequency domain.

For events that pass the selection cut on the observed SNR ρ_{obs} , computed on the specific noise realization, we then find the point $\hat{\theta}$ that minimizes the negative log-likelihood in Eq. (B1) via numerical minimization.¹² Then, we consider the expansion of the likelihood around the ML point $\hat{\theta}$, i.e. $h(\theta) \approx h(\hat{\theta}) + \hat{h}_i \delta\hat{\theta}^i$ with $\delta\hat{\theta}^i = \theta^i - \hat{\theta}^i$. The notation \hat{h}_i indicates the partial derivative evaluated at the point $\hat{\theta}$: $\hat{h}_i \equiv \partial_{\theta_i} h|_{\hat{\theta}}$. We also denote $h(\hat{\theta}) = \hat{h}$.

At first order we get

$$-2 \log \mathcal{L}(\mathcal{D}_{\text{GW}} | \theta) \propto -\delta\hat{\theta}^i \delta\hat{\theta}^j (\hat{h}_i | \hat{h}_j) + 2\delta\hat{\theta}^i (h_0 + n - \hat{h} | \hat{h}_i). \quad (\text{B3})$$

The first term is the usual expansion with a Fisher matrix computed around the ML point, while the second differs from Eq. (B2) because we are expanding the likelihood around $\hat{\theta}$ and not around θ_0 . By definition, the point $\hat{\theta}$ is such that (neglecting overall normalization factors that are not relevant) $-2 \log \mathcal{L}(\mathcal{D}_{\text{GW}} | \hat{\theta}) \approx 0$, so we must have $\mathcal{D}_{\text{GW}} = h_0 + n \approx h(\hat{\theta}) = \hat{h}$, i.e. the second term vanishes. In conclusion, after finding the ML point, in the FIM approximation we can just approximate the likelihood as a multivariate Gaussian centered around $\hat{\theta}$ and with covariance $(\hat{h}_i | \hat{h}_j)^{-1}$.

2. Explicit form of the likelihood approximant

Here we present some expressions of the extended likelihood approximant, which is exact in some subsets of parameters β ; while $\beta = \{d_L, \iota\}$ is the focus of the present work, it is also worth considering other cases.

To begin with, we consider the case $\beta = \{d_L\}$. The waveform parameters are then split as $\theta \equiv \{d_L, \bar{\theta}\}$ and the waveform can be expanded around the ML point as

$$h(d_L, \bar{\theta}) \simeq h(d_L, \hat{\bar{\theta}}) + (\bar{\theta}^i - \hat{\bar{\theta}}^i) \cdot \partial_{\bar{\theta}_i} h(d_L, \bar{\theta})|_{\bar{\theta}=\hat{\bar{\theta}}}. \quad (\text{B4})$$

The approximant obtained with this expansion will encode the effect of noise fluctuations in its width. Replacing this expansion into Eq. (B1) leads to

$$-2 \log \mathcal{L}(\mathcal{D}_{\text{GW}} | d_L, \bar{\theta}) \propto \left(\frac{\hat{d}_L}{d_L} \right)^2 \left[(\delta d_L)^2 \Gamma_{d_L d_L} + 2\delta\bar{\theta}_i \delta d_L \Gamma_{i d_L} + \delta\bar{\theta}_i \Gamma_{ij} \delta\bar{\theta}_j \right], \quad (\text{B5})$$

with

$$\delta d_L \equiv d_L - \hat{d}_L, \quad \delta\bar{\theta}_i \equiv \bar{\theta}^i - \hat{\bar{\theta}}^i. \quad (\text{B6})$$

¹⁰Here and in the following, we drop parameter-independent normalization factors.

¹¹In practice the impact of ignoring this effect on the results of simulations depends on the specific problem, sensitivity, and catalog size, and should be evaluated case-by-case [31].

¹²More specifically, after drawing a specific noise realization over a linear frequency grid, we perform a minimization helped by the fact that we know θ_0 , so the initialization helps the minimizer to converge quickly, and we incorporate physical prior ranges for all parameters.

The prefactor $(\hat{d}_L/d_L)^2$ naturally suppresses the likelihood for small values of d_L , thus making it unnecessary to enforce the prior $d_L > 0$. This version of the likelihood could be useful to treat nearby GW sources, where the Taylor expansion in d_L is less likely to be accurate.

We next consider the case $\beta = \{d_L, \iota\}$, which has been used to produce the results of this paper. We split the waveform parameters as $\theta \equiv \{d_L, \iota, \bar{\theta}\}$, and linearly expand the likelihood in Eq. (B1) only in the subspace of the parameters $\bar{\theta}$. This time the waveform expansion can be written as

$$h(d_L, \iota, \bar{\theta}) \simeq h(d_L, \iota, \hat{\bar{\theta}}) + (\bar{\theta}^i - \hat{\bar{\theta}}^i) \cdot \partial_{\bar{\theta}^i} h(d_L, \iota, \bar{\theta}) \Big|_{\bar{\theta}=\hat{\bar{\theta}}} \quad (\text{B7})$$

To express the final result, we define the polarization-decomposed FIM elements as

$$\Gamma_{ij}^{ab} \equiv \frac{(f_{,i}^a | f_{,j}^b)}{\hat{d}_L^2}, \quad a, b \in \{+, \times\}, \quad (\text{B8})$$

with $f^{a,b}$ defined by

$$\begin{aligned} h(\theta) &= \frac{c_+(\iota)}{d_L} f^+(\bar{\theta}) + i \frac{c_\times(\iota)}{d_L} f^\times(\bar{\theta}), \\ c_+(\iota) &= \frac{1 + \cos^2 \iota}{2}, \quad c_\times(\iota) = \sin \iota. \end{aligned} \quad (\text{B9})$$

where a subscript $_{,i}$ denotes the partial derivative with respect to $\bar{\theta}_i$. The explicit expression for $f^{a,b}$, which is not relevant for the discussion here, can be obtained by comparing the above equations to the full frequency-domain waveform, e.g. Eq. (22) of [33]. We find that the result can be written as

$$\begin{aligned} -2 \log \mathcal{L}(\mathcal{D}_{\text{GW}} | d_L, \iota, \bar{\theta}) &\propto \left(\frac{\hat{d}_L}{d_L} \right)^2 \left[\tilde{\delta} d_L^a \Gamma_{d_L d_L}^{ab} \tilde{\delta} d_L^b \right. \\ &\quad \left. + (\tilde{\delta} \bar{\theta}_i^a \tilde{\delta} d_L^b + \tilde{\delta} \bar{\theta}_i^b \tilde{\delta} d_L^a) \Gamma_{id_L}^{ab} + \tilde{\delta} \bar{\theta}_i^a \Gamma_{ij}^{ab} \tilde{\delta} \bar{\theta}_j^b \right], \end{aligned} \quad (\text{B10})$$

with

$$\begin{aligned} \Gamma_{id_L}^{ab} &\equiv \frac{(f_{,i}^a | f^b)}{\hat{d}_L^3}, \quad \Gamma_{d_L d_L}^{ab} \equiv \frac{(f^a | f^b)}{\hat{d}_L^4}, \\ \tilde{\delta} \bar{\theta}_i^{+, \times} &\equiv \delta \bar{\theta}_i \cdot c_{+, \times}(\iota), \\ \tilde{\delta} d_L^{+, \times} &\equiv \delta d_L \cdot c_{+, \times}(\hat{\iota}) - \hat{d}_L [c_{+, \times}(\iota) - c_{+, \times}(\hat{\iota})]. \end{aligned} \quad (\text{B11})$$

The polarization-decomposed FIM elements $\Gamma_{d_L d_L}^{ab}, \Gamma_{d_L i}^{ab}, \Gamma_{ij}^{ab}$ can be derived from a combination of the usual FIM elements, evaluated at three conveniently chosen values of ι . Using in particular $\iota = \{0, \pi/2, \pi\}$, we have $\Gamma_{IJ}^{++} = 4\Gamma_{IJ}(\iota = \pi/2)$, $\Gamma_{IJ}^{\times \times} = -\{ -[\Gamma_{IJ}(\iota = 0) + \Gamma_{IJ}(\iota = \pi)]/2 + 4\Gamma_{IJ}(\iota = \pi/2) \}$, $\Gamma_{IJ}^{+ \times} + \Gamma_{IJ}^{\times +} = [\Gamma_{IJ}(\iota = 0) - \Gamma_{IJ}(\iota = \pi)]/2$, with $I(J)$ labeling either d_L or $i(j)$ and i, j running over $\bar{\theta}$. While in this paper we use this strategy, we point out that a more

efficient approach would be to compute the FIM for each polarization directly, in which case the computational cost would be identical to that of a single FIM. Using the same argument as in App. B 1, we find that additional corrections to Eq. (B10) at first order in $\delta \hat{\theta}^i$ cancel, so evaluating Eq. (B10) around the maximum likelihood point fully encodes the effects of noise fluctuations.

As a further extension, we also report the result for the case $\beta = \{d_L, \iota, \psi\}$, being ψ the polarization angle. This is relevant for forecasting joint GW+GRB polarization measurements [73]. In this case, the following definitions are needed

$$\Gamma_{ij}^{a\alpha, b\beta} \equiv (f_{,i}^{a\alpha} | f_{,j}^{b\beta}), \quad a, b \in \{+, \times\}, \quad \alpha, \beta \in \{c, s\}, \quad (\text{B12})$$

with

$$\begin{aligned} h(\theta) &= \frac{c_+(\iota)}{d_L} [\cos 2\psi f^{+c}(\bar{\theta}) + \sin 2\psi f^{+s}(\bar{\theta})] \\ &\quad + i \frac{c_\times(\iota)}{d_L} [\cos 2\psi f^{\times c}(\bar{\theta}) + \sin 2\psi f^{\times s}(\bar{\theta})]. \end{aligned} \quad (\text{B13})$$

The likelihood Eq. (B1) in this approximation can be formally written in a way that recalls the previous case

$$\begin{aligned} -2 \log \mathcal{L}(\mathcal{D}_{\text{GW}} | d_L, \iota, \psi, \bar{\theta}) &\propto \left(\frac{\hat{d}_L}{d_L} \right)^2 \left[\tilde{\delta} d_L^{a\alpha} \Gamma_{d_L d_L}^{a\alpha, b\beta} \tilde{\delta} d_L^{b\beta} \right. \\ &\quad \left. + (\tilde{\delta} \bar{\theta}_i^{a\alpha} \tilde{\delta} d_L^{b\beta} + \tilde{\delta} \bar{\theta}_i^{b\beta} \tilde{\delta} d_L^{a\alpha}) \Gamma_{id_L}^{a\alpha, b\beta} + \tilde{\delta} \bar{\theta}_i^{a\alpha} \Gamma_{ij}^{a\alpha, b\beta} \tilde{\delta} \bar{\theta}_j^{b\beta} \right], \end{aligned} \quad (\text{B14})$$

with

$$\begin{aligned} \tilde{\delta} \bar{\theta}_i^{+c} &\equiv \delta \bar{\theta}_i \cdot c_+(\iota) \cos 2\psi \\ \tilde{\delta} d_L^{+c} &\equiv \delta d_L \cdot c_+(\hat{\iota}) \cos 2\hat{\psi} - \hat{d}_L [c_+(\iota) \cos 2\psi - c_+(\hat{\iota}) \cos 2\hat{\psi}], \end{aligned} \quad (\text{B15})$$

and all the other values of $\tilde{\delta} \bar{\theta}_i^{a\alpha}$ and $\tilde{\delta} d_L^{a\alpha}$ for the indexes $a = \{+, \times\}$ and $\alpha = \{c, s\}$ are obtained by replacing $+$ with \times and/or $\cos 2\psi$ with $\sin 2\psi$ in Eq. (B15).

Again, the decomposed FIM matrices can be either computed directly with an adapted code or derived from the usual FIM, evaluated at specific values of ι and ψ (a practical set of values is $\iota = \{0, \pi/2, \pi\}$ and $\psi = \{0, \pi/8, \pi/4\}$).

Finally, we note that this formalism can be extended to all parameters entering the signal amplitude, in particular the sky position, which is crucial for obtaining detailed predictions on localization capabilities.

Appendix C: Population and detector models

1. Populations and detectors

For the GW population we assume $p(m_1, m_2 | \lambda_m) = \mathcal{N}(m_1 | \mu_M, \sigma_M) \mathcal{N}(m_2 | \mu_M, \sigma_M)$ with $\mathcal{N}(x | \mu_M, \sigma_M)$ a

Parameter	Description	Fiducial Value
Cosmology (flat ΛCDM) – λ_c		
H_0	Hubble constant [$\text{km s}^{-1} \text{Mpc}^{-1}$]	70
$\Omega_{m,0}$	Matter energy density	0.3
Rate evolution (Madau–Dickinson) – λ_z		
γ	Slope at $z < z_p$	1.5
κ	Slope at $z > z_p$	5
z_p	Peak redshift	2
Mass distribution (Gaussian) – λ_m		
μ_M	Mean [M_\odot]	1.3
σ_M	Standard deviation [M_\odot]	0.09
EM detection probability – λ_{EM}		
A_0	Amplitude of the flux [erg s^{-1}]	2.7×10^{51}
ι_c	Half-opening of the Gaussian jet profile [deg]	3.27
F_{th}	GRB detector flux threshold [$\text{erg cm}^{-2} \text{s}^{-1}$]	2.7×10^{-7}
Single event parameters – $\{\theta_i\}_{i=1}^{N_{obs}}$		
m_1^{det}	Detector-frame primary mass [M_\odot]	–
m_2^{det}	Detector-frame secondary mass [M_\odot]	–
d_L	Luminosity distance [Gpc]	–
ι	Inclination [deg]	–

Tab. I. Summary of the population hyperparameters λ with their fiducial values, and of the individual event parameters $\{\theta_i\}_{i=1}^{N_{obs}}$ used in the hierarchical model.

Gaussian distribution with fiducial mean and standard deviation $\{\mu_{M,\text{fid}} = 1.3 M_\odot, \sigma_{M,\text{fid}} = 0.09 M_\odot\}$ [74]. The merger rate evolution with redshift in Eq. (A4) is modeled as a Madau–Dickinson (MD) profile [55], $\psi(z; \lambda_z) = (1+z)^\gamma / \{1 + [(1+z)/(1+z_p)]^{\gamma+\kappa}\}$. We use fiducial parameters $\lambda_z = \{\gamma_{\text{fid}} = 1.5, \kappa_{\text{fid}} = 5, z_{p,\text{fid}} = 2\}$. The fiducial values we use are obtained by convolving a MD profile with parameters determined by the Star Formation Rate [55] with a time–delay distribution chosen to be log–flat. We refer to App. A of [33] for details. Inclinations are drawn from a distribution uniform on the sphere, i.e. flat in $\cos \iota$. Since this is the same prior used for the analysis of individual GW events, there is no need to include explicitly this term in the hierarchical likelihood since it will simplify between numerator and denominator [26]. Finally, cosmology is assumed to be described by a flat Λ CDM model with $H_0 = 70 \text{ km s}^{-1} \text{Mpc}^{-1}$, $\Omega_{m,0} = 0.3$.

We consider an observing scenario representative of the best case for the current generation of GW detectors, with a LIGO–Virgo–KAGRA–LIGO India network composed of two LIGO detectors in the US, the Virgo and KAGRA detectors in Italy and Japan, respectively, and a LIGO detector located in India, with A+ sensitivity.¹³ We assume a 100% duty cycle and a SNR threshold of $\rho_{\text{obs}} \geq 12$, where the “observed” SNR is simulated encoding the effects of detector noise.

For the EM detection model, we assume that the jet has a Gaussian-shaped profile, $E(\iota) = E_0 \exp\{-\iota^2/\iota_c^2\}/2$, and we model the detection probability with a threshold on the observed γ –ray flux of each event.¹⁴ This is defined as $F_{\text{GRB}} = \eta E(\iota)/(4\pi d_L^2 T_{90})$, with $\eta = 0.1$ being the radiative efficiency [75, 76], and T_{90} the duration of the period during which 90% of the burst’s energy is emitted, which we assume to be 2 s. Therefore, we define $A_0 = \eta E_0/T_{90}$, and we have explicitly

$$F_{\text{GRB}} = \frac{A_0}{4\pi d_L^2} e^{-\iota^2/\iota_c^2}. \quad (\text{C1})$$

We assume as fiducial values $E_{0,\text{fid}} = 10^{52.73} \text{ erg}$, $\iota_{c,\text{fid}} = 3.27^\circ$ (0.057 rad), obtained by a multi-messenger analysis of GW170817 [56]. We will consider an event as detected if the flux exceeds the Fermi–GBM–like sensitivity of $F_{\text{th}} = 2 \times 10^{-7} \text{ erg cm}^{-2} \text{s}^{-1}$ [54].¹⁵ In conclusion, we define $\lambda_{\text{EM}} = \{A_0, \iota_c, F_{\text{th}}\}$, and we have

$$P(\text{det}_{\text{EM}} | \iota, d_L, A_0, \iota_c) = \begin{cases} 1 & \text{if } F_{\text{GRB}}(\iota, d_L, A_0, \iota_c) \geq F_{\text{th}} \\ 0 & \text{otherwise} \end{cases}. \quad (\text{C2})$$

Tab. I summarizes the population hyperparameters and individual event parameters used in the paper.

¹³Specifically, we use the `AplusDesign` public sensitivity curve for the three LIGO detectors, `avirgo_05low_NEW` for Virgo, and `kagra_80Mpc` for KAGRA [53], available at <https://dcc.ligo.org/LIGO-T2000012/public>.

¹⁴We assume the uncertainty in the measurement of the flux to be negligible.

¹⁵This model corresponds to the one used in [77, 78], with the slight simplification that they introduce a distribution on the peak luminosity E_0 , while here we consider it fixed. We have checked that the scaling of Θ_{max} with redshift is consistent among the two.

2. Mock dataset

We simulate the GW likelihood for each joint detection by using the likelihood approximant described in App. B. We use the public software `gwfast` [33, 41] for the evaluation of the FIM, and we extract samples from the posterior given by Eq. (B10) multiplied by a prior (denoted by $\pi(\theta_i) \forall i$) flat in $\cos(\iota)$ with $\iota \in [0, \pi]$, flat in detector-frame masses, and flat in the other variables. This reproduces actual data-analysis choices. We use the affine-invariant MCMC sampler `zeus` [79, 80]. We assume that the sky position is known and fixed to the host galaxy, and the GPS time of detection is known.¹⁶

For the EM data, we assume a Gaussian likelihood with standard deviation $\sigma_z = 10^{-3}$. We simulate a redshift measurement by drawing, for each event that passes the selection cut in the GW and EM, an “observed” value from this likelihood.

In summary, this procedure yields a set of samples from the posterior $p(\theta_i | \mathcal{D}_{\text{GW}}^i) \propto \mathcal{L}(\mathcal{D}_{\text{GW}}^i | \theta_i) / \pi(\theta_i)$ for each GW event and a redshift measurement, as in data analysis of real events.

Finally, to estimate the selection effect $P(\text{det} | \lambda)$ in Eq. (1) we use reweighted Monte Carlo integration [81, 82]. We generate a large injection set and apply the same selection cut used for constructing the catalog for GW observations, while crucially no EM selection is applied to the injections, as the EM selection probability will be inferred during inference.

3. Hierarchical inference

Starting from the mock data, we sample Eq. (1) in the high-dimensional space of $\lambda, \{\theta_i\}$ using PyMC [57] and the Hamiltonian Monte Carlo [58] based scheme NUTS [59]. This choice is dictated by the necessity of accurately exploring the posterior distribution of individual GW events in the corner of the parameter space at small inclination which is preferentially selected by the EM detection probability. Using standard approaches that rely on Monte Carlo integrals over existing posterior samples [26] would either result in numerically unreliable results or require an unreasonably large amount of individual posterior samples. In our implementation, prior to inference we instead fit a continuous interpolant of the individual GW likelihoods with a Gaussian Mixture Model over posterior samples [83], from which we can continuously resample at inference time.

¹⁶To limit the computational cost, we also fix the phase at coalescence, polarization angle, and tidal deformabilities. We checked that this does not lead to underestimation of the uncertainty on the masses, distance, and inclination. On the contrary, fixing the spins or neglecting them would lead to substantial underestimation of the uncertainty on the detector-frame mass.